Ballistic electron transport in Au films

X. Liu, R. Stock, and W. Rudolph*
Department of Physics and Astronomy, University of New Mexico, 800 Yale Blvd. NE., Albuquerque, New Mexico 87131, USA
(Received 1 March 2005; revised manuscript received 20 June 2005; published 29 November 2005)

Femtosecond transient reflectivity measurements on gold films revealed damped oscillations, which are attributed to anisotropic ballistic electron motion and reflection at the film boundaries. A theoretical model based on a modified Fermi-liquid theory can explain the observed oscillation periods as a result of ballistic transport in directions determined by the actual shape of the Fermi surface of Au.

DOI: 10.1103/PhysRevB.72.195431 PACS number(s): 78.47.+p, 73.20.Mf, 73.50.Gr, 72.15.Lh

I. INTRODUCTION

Femtosecond studies of nonequilibrium electrons and phonons and their interaction in metals have been the subject of numerous studies in the past two decades. Fundamental processes in the excited electronic system are important for the thermal and electronic properties of metals and surface processes as, for example, desorption and phase transitions. Most of the experimental studies were performed using pump-probe reflection/transmission[1–5] and two-photon photoemission experiments.[6,7] It was found that a combination of Coulomb screening and the Pauli exclusion principle can lead to electron-electron scattering times on the order of a few hundred femtoseconds, slowing down the thermalization of the electron gas. This necessitated the modification of the two-temperature model[8] that assumed an instantaneous formation of a thermalized electron gas of certain temperature T_e, which then interacts with the phonons.

Carrier transport was studied in metal films excited at the front surface and probed at the front and back surface[4,9] with femtosecond time resolution. From the delayed rise of the signal at the back surface a transport velocity v on the order of the Fermi velocity independent of the film thickness d was found for $d \leqslant 400$ nm. This was interpreted as ballistic transport of nonthermal electrons. Because of the small absorption lengths d_s of metal films (for example, Au at 1.5 eV: $d_s \approx 13$ nm) transport of the excitation perpendicular to the surface has to be taken into account for the interpretation of measurements of subpicosecond particle dynamics near the material surface; see, for example, Refs. 10–12.

The existence of a ballistic transport component suggests the possibility that a fraction of the initial nonthermal electrons may be reflected at the back surface of the film and propagate to the front surface where they are reflected again. This would continue over the "lifetime" of ballistic electrons. For film thicknesses small enough, a few roundtrips should manifest themselves in an oscillatory behavior of the transient reflectivity signal in a pump-probe experiment. In this paper we show experimental evidence of the existence of this kind of periodic unhindered particle transport. A theoretical model based on a modified Fermi-liquid theory and the specific Fermi surface geometry of Au is in good agreement with the observed transient reflectivity signal.

II. EXPERIMENT

For our studies of ballistic transport in Au films we chose a degenerate pump-probe experiment at photon energies of $\hbar\omega = 1.55$ eV. The band structure of Au together with the pump and probe transitions are shown in Fig. 1. The pump excites intraband transitions of electrons near the Fermi level. In addition to these intraband transitions the probe can also test transitions from d bands to states below the Fermi level emptied by the pump. The excitation and probing was performed at the angle for the surface plasmon (SP) resonance for two reasons. First, it allows an efficient excitation and sensitive probing of the induced material changes.[2] Second, the induced reflectivity change

$$\frac{\Delta R}{R} = \frac{\partial \ln R}{\partial \varepsilon'}\Delta\varepsilon' + \frac{\partial \ln R}{\partial \varepsilon''}\Delta\varepsilon'' \qquad (1)$$

is mainly determined by the change of the imaginary part of the dielectric constant, $\Delta\varepsilon''$. The contribution of the real part, $\Delta\varepsilon'$, can be neglected since $72 \geqslant (\partial R/\partial\varepsilon'')/(\partial R/\partial\varepsilon') \geqslant 40$ for film thicknesses 30 nm $\leqslant d \leqslant$ 45 nm, and since $|\Delta\varepsilon'| < |\Delta\varepsilon''|$ as will be explained below.

The experimental setup is shown in Fig. 2. Pulses from a 22-fs Ti:sapphire laser ($\hbar\omega_0 = 1.55$ eV) were used to excite and probe films with thicknesses of 30 nm and 45 nm. The films were deposited on a BK-7 glass slide by e-beam evaporation. The slide was attached to the hypotenuse of a BK-7 prism with an index-matching oil. Pump and probe were displaced vertically (along x) before the focusing lens ($f \approx 12.5$ cm) and were incident at a common spot ($A \approx 1200\ \mu\text{m}^2$) at the SP resonance angle in the Kretschmann[13] configuration. Pump and probe beams were

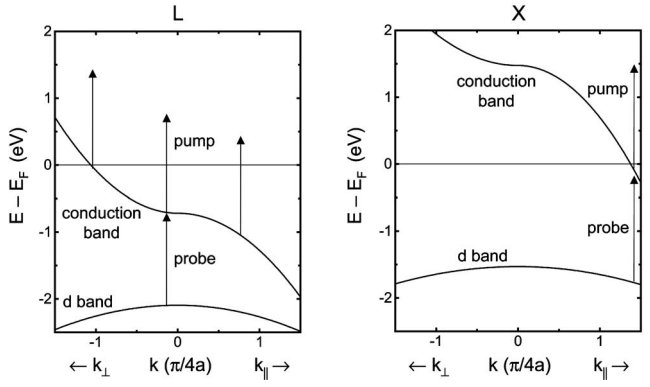

FIG. 1. Band structure of Au and transitions relevant for excitation and probing at $\hbar\omega \approx 1.55$ eV near the L and X point.

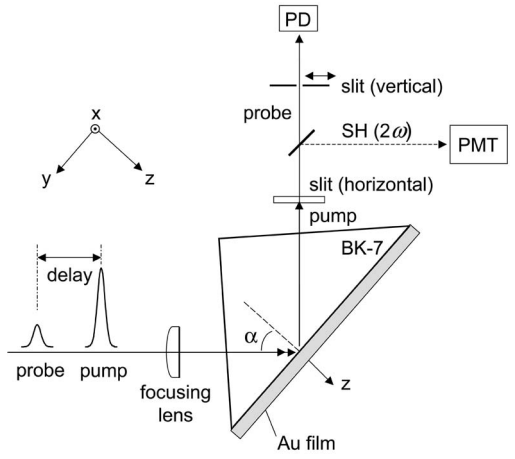

FIG. 2. Experimental pump-probe setup. Excitation and probing is at the surface plasmon resonance using the Kretschmann configuration.

chopped at different frequencies and the signal was detected at the sum frequency. Induced reflectivity changes of the order of 10^{-5} could readily be measured. A horizontal slit blocked the pump beam after reflection. A vertical slit in the path of the reflected probe selected the beam component probing at the SP resonance. A prism sequence between the laser oscillator and the pump-probe setup allowed us to compensate the cumulative group velocity dispersion up to the Au film. We also measured the cross-correlation of pump and probe pulses simultaneously with the transient reflectivity by detecting the noncollinear second-harmonic (SH) signal produced at the Au surface.

Figure 3 depicts the transient reflectivity result obtained with the 45-nm film. The measured cross-correlation of pump and probe is shown for comparison. The correlation width of 34 fs is somewhat larger than what is expected from the pulse duration. This discrepancy can be explained by the noncollinear beam overlap on the sample, which was necessary to separate pump and probe after reflection. An initial fast decay of the transient reflectivity is followed by a damped oscillation. The oscillation period is found to be about 107 fs and about 70 fs for the 45-nm film and the 30 -nm film, respectively. Assuming transport perpendicular to the film surface, this corresponds to an effective velocity of about 0.85×10^6 m/s, which is of the same order of magnitude as the Fermi velocity $v_F\approx1.4\times10^6$ m/s.

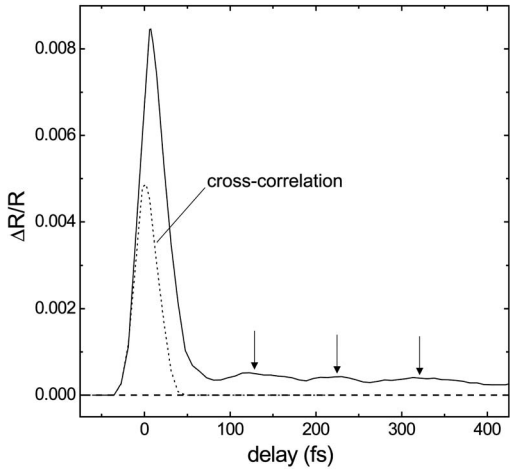

FIG. 3. Measured transient reflectivity of a 45-nm Au film probed at the surface-plasmon resonance. The dash-dotted line shows the background-free cross-correlation of pump and probe for comparison.

III. THEORETICAL MODEL

To model the experiment we need to study the spatiotemporal evolution of excited electrons in the gold film and its effect on the transient reflectivity in the first few hundred fs after excitation. This is the time range where the electrons have not yet thermalized and the material response cannot be characterized by an electron temperature T_e. In our model we divide the electron distribution into two parts—a thermalized Fermi sea and a nonequilibrium distribution acting as a perturbation. This is justified given the relatively small density of excited electrons ($\sim2\times10^{19}$ cm^{-3}) compared to the total electron density of $\sim6\times10^{22}$ cm^{-3}. Transport is only considered for the nonthermal electrons on the time scale of interest here. The film acts as a Fabry-Perot etalon for the probe pulse. The transient reflectivity ΔR at the SP resonance is obtained by dividing the film into N slices and calculating the optical stack matrix. Each slice is characterized by a local dielectric constant that is governed by the spatiotemporal evolution of the carrier density.

The pump-pulse induced change of the imaginary part of the dielectric function can be divided into two contributions,

$$\Delta\varepsilon'' = \Delta\varepsilon''_{cb} + \Delta\varepsilon''_{ir}, \tag{2}$$

where $\Delta\varepsilon''_{cb}$ results from intraband transitions in the conduction band and $\Delta\varepsilon''_{ir}$ from interband transitions.

To describe the intraband transitions of quasifree electrons we invoke Drude theory

$$\Delta\varepsilon''_{cb}(t) = \frac{\varepsilon''_{cb}}{\gamma}\Delta\gamma(t), \tag{3}$$

where γ is the total scattering rate, which is the sum of the electron-(acoustic) phonon (ep) and electron-electron (ee) scattering rate $\gamma=\gamma_{ep}+\gamma_{ee}$. The associated change of the real part of the dielectric function $|\Delta\varepsilon'_{cb}/\Delta\varepsilon''_{cb}| \approx 2(\gamma/\omega)^2|\varepsilon'_{cb}/\varepsilon''_{cb}|<1$ for $\varepsilon_{cb}\approx-23-i0.77$ and $\gamma\approx10^{14}$ s^{-1}. Its contribution to the measured signal [cf. Eq. (1)] can thus be neglected when working at the SP resonance as indicated earlier.

In the short time scale of interest here, $\Delta\gamma(t)\approx\Delta\gamma_{ee}(t)$ is controlled by electron-electron scattering. This change in the average scattering rate is due to energy transfer from the nonequilibrium electrons to the electrons in the Fermi sea, which leads to a change in the electron temperature $\Delta T_e(t)$. The energy deposition by the pump pulse has a noninstantaneous effect on the average scattering rate, leading to a delayed rise of the reflectivity signal[3,5] that is proportional to $\Delta\varepsilon''_{cb}$. For short time scales, before electron-phonon relaxation becomes important, the reflectivity signal due to intraband transitions can be described by

$$\Delta R_{cb}(t) = A_0 \Phi(t)(1 - e^{-t/\tau_e}) \otimes C(t), \tag{4}$$

where $\Phi(t)$ is the Heaviside step function and $\otimes C(t)$ stands for the convolution with the cross-correlation function of pump and probe.[3] The parameter $\tau_e \approx 35$ fs is an effective electron thermalization time that was obtained from a fit of Eq. (4) to the data presented in Fig. 3 of Ref. 5. According to Eq. (4) the signal increases to reach a plateau with a time constant that is somewhat longer than what one would expect from a simple convolution of the absorbed pump energy and $C(t)$. We can determine the amplitude factor A_0 from a fit to the plateau reached after 400 fs in our experiments.

The contribution from interband transitions to the transient reflectivity change, $\Delta R_{ir}(t)$, which is responsible for the oscillatory peak of the reflectivity signal as can be seen in the next section, can be calculated from the optical stack matrix. This matrix is the product of the optical matrices of the individual film slices whose elements are determined by $\Delta\varepsilon''_{ir}(t,z)$. To obtain $\Delta\varepsilon''_{ir}(t,z)$ we will apply a one-dimensional transport model for the nonequilibrium carrier density.

The change in the interband part of the dielectric constant, $\Delta\varepsilon_{ir}$, originates from transitions from the low lying d bands to the empty states created in the conduction band around the X and L point (cf. Fig. 1). The resulting change in the imaginary part, $\Delta\varepsilon''_{ir}$ at probe frequency ω, can be described in the constant matrix element approximation[14,15] by

$$\Delta\varepsilon''_{ir}(t,z) = -\frac{2h^2}{3m^2\omega^2} \sum_{j=X,L} |P|^2 r_j \int_{E_{j1}}^{E_{j2}} \mathcal{D}_j(E,\hbar\omega)\Delta\rho(E,z,t)dE, \tag{5}$$

where m is the electron mass, P is the transition matrix element, r_L and r_X are the relative transition strengths, $\mathcal{D}_j(E,\hbar\omega)$ is the energy distribution of the joint density of states, and $\Delta\rho = \rho - \rho_{eq}$ is the difference of the actual and the equilibrium quasiparticle distribution. All energies E are measured from the Fermi energy E_F and taken positive. The integration limits define the energy regions over which $\Delta\rho(E)$ is probed for the different transitions. For the transition near the L and X point this energy interval is (0.58 eV, 1.55 eV) and (0.24 eV, 1.55 eV) (Ref. 16), respectively. The integration limit of 1.55 eV is determined by the pump photon energy. The relative strengths of the transition matrix elements, $r_X/r_L \simeq 0.37$, see Ref. 14. The evolution of the nonthermal electron distribution involves electron and hole scattering. For example, a collision of a nonthermal electron with an electron from the Fermi sea will produce two excited electrons and one hole. We will therefore use the terminology "quasiparticle" or "particle" in equations used to determine $\Delta\varepsilon''_{ir}$.

To discuss the contribution of the interband transition to the signal we need the evolution of the nonthermal quasiparticle distribution $\Delta\rho(E,z,t)$ affected by transport, *ee* scattering, and the excitation. Because the film thickness is much smaller than the probed spot diameter, the transport can be considered one dimensional. We assume that the pump initially creates a nonuniform electron distribution governed by the spatial intensity distribution in the film, $f(z)$, and an energy distribution $g(E)$ with $g=1$ for $0 \leqslant E \leqslant \hbar\omega_0$ and $g=0$ otherwise. At the SP resonance, the optical pulse creates a nonequilibrium electron distribution that initially peaks at the film-air interface before it propagates.

Within the framework of one-dimensional transport, the quasiparticles can move in two opposite directions ($+z$ and $-z$) with equal probability. We will model two different transport scenarios: (i) isotropic ballistic transport where each direction is equally probable and the z component of the velocity vector v_z is taken from an interval $(-v_0, v_0)$, and (ii) transport in preferred directions with $v_z = \pm v_t$. Here v_t is an effective transport velocity along the z direction. For the case of isotropic transport we use $v_0 = v_F$, where $v_F \approx 1.4$ nm/fs is the Fermi velocity of Au. Each scattering event creates new particles at certain energies. The distribution of quasiparticles moving in $+z$ direction, $\Delta\rho_+(E,z,t,v_z)$, can be described by

$$\frac{\partial}{\partial t}\Delta\rho_+ = \left[v_z \frac{\partial}{\partial z} - \frac{1}{\tau_{ee}(E)} \right] \Delta\rho_+ + \frac{1}{2}\kappa P(t) f(z) g(E) h(v_z) + 3\int_E^\infty \frac{\Delta\rho_+(E') + \Delta\rho_-(E')}{\tau_0}(E' - E)dE'. \tag{6}$$

A similar equation holds for the particle density moving in the opposite direction, $\Delta\rho_-(E,z,t,-v_z)$. The parameter $\tau_0^{-1} \approx 0.05$ fs^{-1} eV^{-2} is a characteristic scattering constant[17] from Fermi-liquid theory according to which the scattering rate of hot electrons was approximated by $\tau_{ee}^{-1}(E) \approx E^2/\tau_0$. The quantity κ is the absorption coefficient of Au, and $P(t)$ is the excitation photon flux density. The distributions $h(v_z) = 1/v_t$ and $h(v_z) = \delta(v_z - v_t)$ apply to case (i) and case (ii), respectively.

The last term on the right-hand side of Eq. (6) describes the filling of states with energy E by scattering of particles out of states with energy $E' > E$, which was derived in Ref. 18 and implemented in this form in Refs. 19 and 4. We assume that the excited quasiparticles travel ballistically until they are scattered out of the energy window probed by transitions from the d band to the conduction band. At this point they join the sea of thermalized particles whose average effect is described by $\Delta\gamma(t)$ and $\Delta\varepsilon''_{cb}$. The effect of reflection of quasiparticles reaching the film boundaries is taken into account. We neglected the energy dependence of v because the major contribution to the observable ballistic transport originates from electrons with energies near $E_{min} \approx 0.24$ eV as will be explained below. We also neglected electron-phonon scattering in Eq. (6). According to Ref. 4, within our time scale of interest, the average *e-p* energy relaxation time $\langle\tau_{ep}\rangle \geqslant 1.5$ ps. The effect of momentum relaxation due to the quasielastic scattering will be discussed in the next section.

The total particle density needed in Eq. (5) to compute $\Delta\varepsilon''_{ir}(t,z)$ is obtained from $\Delta\rho(E,z,t) = \int[\Delta\rho_+(E,z,t,v) + \Delta\rho_-(E,z,t,v)]dv$. The dielectric constant $\Delta\varepsilon''_{ir}(t,z_i)$ was used to calculate the optical matrix of a film slice at $z = z_i$. A slice thickness of 1 nm turned out to be sufficient to adequately sample the film.

We checked whether the excitation and probing at the surface-plasmon resonance leads to additional temporal

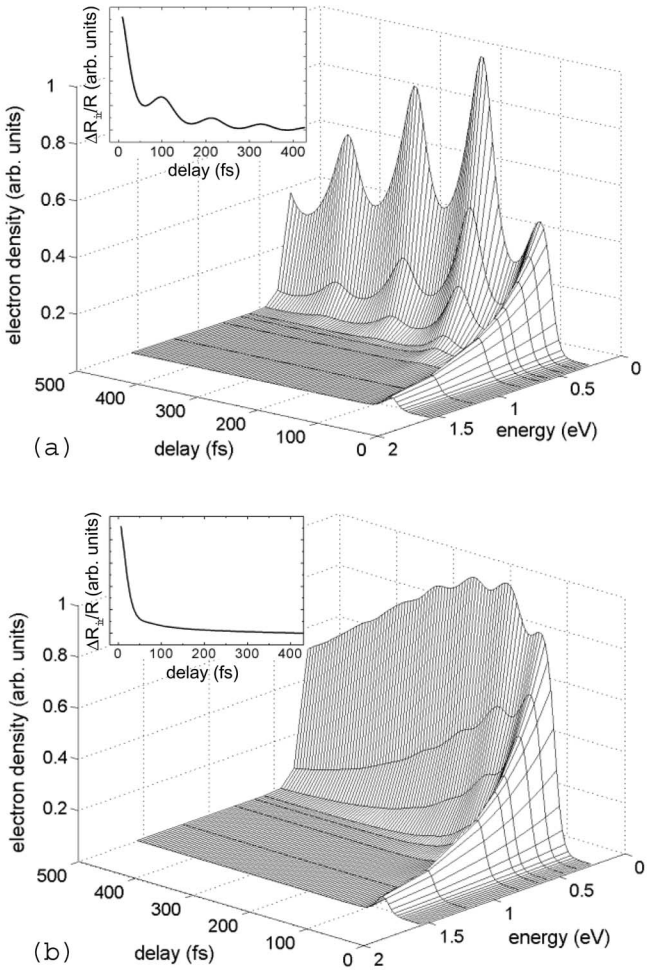

FIG. 4. Calculated density of quasiparticles at the Au-air interface of the 45-nm film as a function of energy and time after excitation. (a) Directed transport with an effective transport velocity along the z direction $v_t=0.85\times10^6$ m/s, (b) isotropic transport. The insets show the calculated transient reflectivity signal ($\Delta R_{ir}/R$).

smearing due to the interplay of the spectral and angular properties of the plasmon resonance and the focused fields of pump and probe. It turns out that the resulting effects are negligible for pulses as short as 10 fs and our beam focusing geometry.

IV. RESULTS AND DISCUSSION

Figure 4 shows the quasiparticle density at the Au-air interface of the 45-nm film as a function of time and energy calculated from Eq. (6) for isotropic and directed ballistic transport. The insets show the resulting transient reflectivity signals ($\Delta R_{ir}/R$) obtained from the optical stack matrix.

Obviously, an oscillatory behavior is sustained over several hundreds of fs for the directed transport [Fig. 4(a)]. The oscillations are most pronounced for quasiparticles in low-energy states. This is a manifestation of the Pauli exclusion principle. Quasiparticles near the Fermi level have long scattering times due to the lack of empty states they can scatter into. Therefore, as shown in Fig. 1, transitions near the X point that probe particle states of small energy (0.24 eV) are particularly sensitive to ballistic transport. Only a small contribution to the observed modulation is expected from quasiparticles with larger energies. This is despite the fact that the L-point transitions carry a larger weight in the integral in Eq. (5).

The amplitude of the modulation of the particle density at the lowest probed energies still increases after the pump pulse. The population of the energy levels described by the last term in Eq. (6) is responsible for this behavior. For isotropic transport, the modulation is much weaker [Fig. 4(b)] and not visible in the transient reflectivity signal. Since all velocity components v_z from the interval $(-v_0,v_0)$ are equally probable, the modulation period is determined by the leading front of the electron packet that travels with $v_z\approx v_0$. It is evident that the modulation observed in our experiment cannot be explained with isotropic transport.

To answer the question as to what can be the physical origins of a directed ballistic transport, we need to evaluate the Fermi surface of Au. Due to the fact that the principal contribution to the observable ballistic transport originates from electrons with energies close to the Fermi level, a discussion of transport based on the Fermi surface $E(\vec{k})=E_F$ should be a good approximation. From the semiclassical model of electron transport, the ballistic transport velocity is perpendicular to the Fermi surface, $\vec{v}(\vec{k})=(1/\hbar)\nabla_k E(\vec{k})$. Only for ideal parabolic bands is the surface of constant energy spherical and isotropic transport can be expected. Thus the nonspherical shape of the Fermi surface of Au suggests highly anisotropic ballistic electron transport. Particle transport is most preferred in directions perpendicular to regions, where the curvature of the Fermi surface is small (close to zero) and the velocity vectors $\vec{v}(\vec{k})$ of adjacent k states point in a similar direction. This translates into a relatively large number of particles occupying adjacent states that move in nearly the same direction with similar speed.

Such anisotropic transport due to nonspherical Fermi surfaces was predicted[20] and experimentally observed in semimetals[21] and metals.[22] In these experiments, carriers were excited on one side of a platelet in the near field of an optical fiber tip. The potential distribution at the opposite site of the plate was probed by a metal point-contact while the fiber tip was raster-scanned. As part of a detailed analysis of transport measurements on metal-semiconductor interfaces,[23] preferred directions of ballistic transport in Au were retrieved from the actual shape of the Fermi surface.[24]

Au films produced by evaporation usually consist of grains whose average size is on the order of the film thickness d, if $d<50$ nm, with the $\langle111\rangle$ axis perpendicular to the substrate surface.[27] The orientation of the Fermi surface relative to the film and the areas of low curvature (regions A and B) with the corresponding directions of $\vec{v}$ are illustrated in Fig. 5. The regions A and B indicate areas within which the direction of $\vec{v}$ varies less than $\pm10°$ and the magnitude by less than 10% with respect to the mean values $v_A\approx1.5$ nm/fs and $v_B\approx1.15$ nm/fs, respectively.[28,29]

The location of the main regions contributing to the directed ballistic transport are labelled $A1$, $A2$, and $B1$. The corresponding velocity vectors include an angle with the

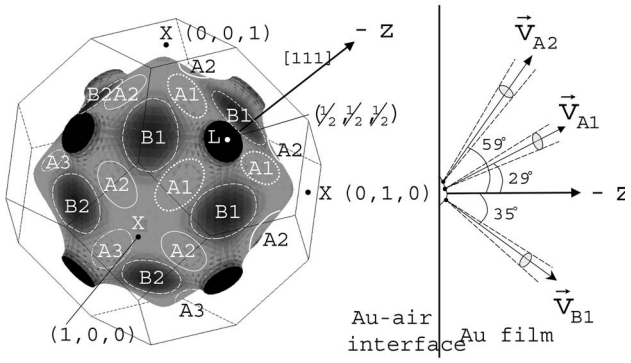

FIG. 5. Left: Velocity distribution on the Fermi surface of Au (adapted from Refs. 25 and 26). Right: The main components of ballistic transport relative to the film.

$\langle 111 \rangle$ axis of $\sim \pm 29°$, $\sim \pm 59°$, and $\sim \pm 35°$, respectively; thus $v_{zA1} \approx \pm 0.87 v_A$, $v_{zA2} \approx \pm 0.52 v_A$ and $v_{zB1} \approx \pm 0.82 v_B$. Assuming equal quasiparticle population, $\Delta\rho$, the relative weight of these three velocity groups is approximately $A1:A2:B1 = 1:1:1.5$, and they comprise about 55% of the total population.

The other A and B regions, $A3$ and $B2$, contribute to the transport with components nearly parallel to the film surface with $\alpha_{A3} \approx 81°$ and $\alpha_{B2} \approx 90°$ resulting in $v_{zA3} \approx 0.24$ nm/fs and $v_{zB2} \approx 0$. In our time scale of interest ($\sim$400 fs) these components will not result in a modulation of the reflectivity signal. We therefore lump their contribution to the signal into the background [cf. Eq. (4)]. The same is true for the electrons from areas on the Fermi surface outside the marked regions ($\approx 20\%$). The strong curvature and the various possible orientations give rise to a small isotropic transport component.

In summary, the actual shape of the Fermi surface suggests directed ballistic transport that consists of three components with velocity projections v_{zA1}, v_{zA2}, and v_{zB1}. This situation was simulated with Eq. (6) and the resulting quasiparticle distribution $\Delta\rho(E,z,t)$ was inserted into Eq. (5) to obtain $\Delta\varepsilon''_{ir}(t,z)$. The transient reflectivity due to $\Delta\varepsilon''_{ir}$ was then calculated from the optical stack matrix of the film and convoluted with the probe pulse. The results for the two film thicknesses together with the measurements are shown in Fig. 6. The intraband contribution, Eq. (4), can explain the offset after the modulations are damped. There will be an additional small time-dependent contribution from $\Delta\varepsilon''_{cb}$ to the signal during the first $\sim$50 fs, which is within the first peak of the modulation. The modulation periods will not be affected by the intraband contributions.

The initial peak observed in the experiment is a combination of the coherence spike and the extremely fast relaxation of quasiparticles with the highest energies. Due to the complicated nature of the origin of the coherence spike, no attempt was made to fit its amplitude exactly. Within experimental error the calculated modulation periods are in good agreement with the observations. The observed modulation is the result of the superposition of three velocity components. Using the first modulation period we can determine an effective velocity normal to the film surface of $\sim$0.88 nm/fs, which compares well with the experimental value of $\sim$0.85 nm/fs.

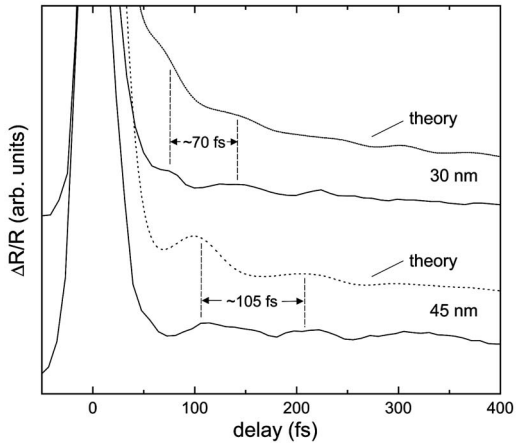

FIG. 6. Comparison of the experiment and modeling results $[\Delta R_{ir}/R \otimes P(t)]$. The curves are displaced vertically for clarity.

Although e-p scattering contributes very little to the energy relaxation of the excited electrons in the time scale of interest, the effect of momentum change on the ballistic transport needs discussion. An average quasiparticle-phonon scattering time of about 90 fs was estimated for Au (see Refs. 4 and 19). This corresponds to an e-p mean-free-path of $\sim$130 nm for quasiparticles moving with the Fermi velocity. Thus the quasiparticle transport in Au is mostly ballistic for propagation lengths of the order of 100 nm. This is also in agreement with observations on single- and polycrystalline Au films.[30,31] Thus the first oscillation period observed with our 30-nm and 45-nm Au films is dominated by ballistic transport. For longer times ($\sim$150 fs–400 fs) the momentum changing collisions will lead to "attenuated ballistic transport,"[9] causing additional damping and smearing of the oscillations in our case.

Another possible effect that reduces the modulation contrast is imperfect reflection at the film boundaries both with respect to amplitude and direction, with the latter due to surface corrugations, for example. This would particularly affect the ratio of the second and third peak. On the other hand a certain roughness of the Au-air interface where the quasiparticles are initially excited will lead to a thinner effective skin depth.[32] This in turn would lead to an enhancement of the amplitude contrast.

Since we did not attempt to fit the actual amplitudes of the recurring signals and used only the first periods to estimate the transport velocity, we did not include quasielastic scattering and possible surface scattering effects in our model.

The reflectivity levels off after about 400 fs at $\Delta R/R \approx 1 \times 10^{-4} (\approx 3 \times 10^{-4})$ for the 30-nm (45-nm) film. This plateau is determined by the rise of the average electron temperature $\Delta T_e \approx 100$ K, and thus $\Delta R \approx \Delta R_{cb}$.[5] The resulting reflectivity change $\Delta R_{cb}/R \approx (\partial R/\partial \varepsilon''_{cb})(\varepsilon''_{cb}/R)(\Delta\gamma_{ee}/\gamma)$. Using the results of Ref. 33 for the temperature-dependent part of the ee-scattering rate $\gamma_{ee}(T)$ and the total scattering rate γ, we find $\Delta\gamma_{ee}/\gamma \approx (0.2 \ldots 1) \times 10^{-3} \Delta T/T$. This yields for $\Delta R_{cb}/R = (0.4 \ldots 2) \times 10^{-4} [(1.3 \ldots 6.5) \times 10^{-4}]$ for the 30-nm (45-nm) film when probed at the plasmon resonance, which is in reasonable agreement with the measurements (cf. Fig. 3).

V. SUMMARY

In summary, transient reflectivity experiments on Au films at the surface-plasmon resonance showed damped oscillations in the first few hundred femtoseconds. A theoretical model taking into account anisotropic ballistic transport due to the nonspherical shape of the Fermi surface of Au, quasiparticle scattering, and the optical film response can explain the oscillatory behavior of the reflection signal. The ballistic signal is dominated by electrons near the Fermi level that have scattering times of several hundred fs. The observed modulation period of the reflectivity signal in the first few hundred fs after excitation is the result of the superposition of three ballistic transport components.

One component of our theoretical description is Fermi-liquid theory for the quasiparticle scattering. More sophisticated theoretical approaches exist (see, for example, Ref. 34) that can be combined with our transport model. Since these models predict relatively long scattering times similar to those from Fermi-liquid theory for quasiparticles near the Fermi level, the expected modifications of the transient reflection signal are minor.

ACKNOWLEDGMENTS

The authors would like to thank M. O'Brien, T. Rotter, and Y. Zhao for help with the preparation of the Au samples. We thank D. Emin, N. Kenkre, D. Dunlap, and M. Hasselbeck for stimulating and helpful discussions. We also thank G. Manfredi and P.-A. Hervieux for sending us their recent paper[35] on Vlasov simulations of ballistic transport to explain our data.[36] This work was supported in part by ONR (Grant No. N-00014-95-1315), ARO (Grant No. W911NF-05-1-0507, and NSF (Grant No. ECS-0100636 and Grant No. DGE-0114319).

*Electronic address: wrudolph@unm.edu

[1] R. W. Schoenlein, W. Z. Lin, J. G. Fujimoto, and G. L. Eesley, Phys. Rev. Lett. **58**, 1680 (1987).
[2] R. H. M. Groeneveld, R. Sprik, and A. Lagendijk, Phys. Rev. Lett. **64**, 784 (1990).
[3] C.-K. Sun, F. Vallée, L. H. Acioli, E. P. Ippen, and J. G. Fujimoto, Phys. Rev. B **50**, 15337 (1994).
[4] C. Suárez, W. E. Bron, and T. Juhasz, Phys. Rev. Lett. **75**, 4536 (1995).
[5] N. DelFatti, R. Bouffanais, F. Vallée, and C. Flytzanis, Phys. Rev. Lett. **81**, 922 (1998).
[6] W. S. Fann, R. Storz, H. W. K. Tom, and J. Bokor, Phys. Rev. Lett. **68**, 2834 (1992).
[7] J. Cao, Y. Gao, H. E. Elsayed-Ali, R. J. D. Miller, and D. A. Mantell, Phys. Rev. B **58**, 10948 (1998).
[8] S. I. Anisimov, B. L. Kapeliovich, and T. L. Perel'man, Sov. Phys. JETP **39**, 375 (1974).
[9] S. D. Brorson, J. G. Fujimoto, and E. P. Ippen, Phys. Rev. Lett. **59**, 1962 (1987).
[10] M. Aeschlimann, M. Bauer, and S. Pawlik, Chem. Phys. **205**, 127 (1996).
[11] E. Knoesel, A. Hotzel, and M. Wolf, Phys. Rev. B **57**, 12812 (1998).
[12] M. Lisowski, P. A. Loukakos, U. Bovensiepen, J. Sthler, C. Gahl, and M. Wolf, Appl. Phys. A **78**, 165 (2004).
[13] H. Raether, *Surface Plasmons on Smooth and Rough Surfaces and on Gratings* (Springer-Verlag, Berlin, 1988).
[14] R. Rosei, F. Antonangeli, and U. M. Grassano, Surf. Sci. **37**, 689 (1973).
[15] R. Rosei, Phys. Rev. B **10**, 474 (1974).
[16] R. Stock, MS thesis, University of New Mexico, 2001.
[17] R. H. M. Groeneveld, R. Sprik, and A. Lagendijk, Phys. Rev. B **51**, 11433 (1995).
[18] R. H. Ritchie, J. Appl. Phys. **37**, 2276 (1966).
[19] G. Tas and H. J. Maris, Phys. Rev. B **49**, 15046 (1994).
[20] Y. V. Sharvin and L. M. Fisher, JETP Lett. **1**, 152 (1965).
[21] J. Heil, M. Primke, K. U. Wurz, and P. Wyder, Phys. Rev. Lett. **74**, 146 (1995).
[22] J. Heil, M. Primke, A. Böhm, P. Wyder, B. Wolf, J. Major, and P. Keppler, Phys. Rev. B **54**, R2280 (1996).
[23] W. J. Kaiser and L. D. Bell, Phys. Rev. Lett. **60**, 1406 (1988).
[24] F. J. Garcia-Vidal, P. L. de Andres, and F. Flores, Phys. Rev. Lett. **76**, 807 (1996).
[25] C. Lehmann, S. Sinning, P. Zahn, H. Wonn, and I. Mertig, http://www.phy.tu-dresden.de/~fermisur/
[26] P. Zahn (private communication).
[27] C. V. Thompson, Annu. Rev. Mater. Sci. **30**, 159 (2000).
[28] J. Graefenstein, I. Mertig, E. Mrosan, V. N. Antonov, and VL. N. Antonov, Phys. Status Solidi B **147**, 575 (1988).
[29] T.-S. Choy, J. Naset, J. Chen, S. Hershfield, and C. Stanton, Bull. Am. Phys. Soc. **45**, L36 42 (2000).
[30] T. Juhasz, H. E. Elsayed-Ali, G. O. Smith, C. Suárez, and W. E. Bron, Phys. Rev. B **48**, R15488 (1993).
[31] J. Hohlfeld, J. G. Müller, S.-S. Wellershoff, and E. Matthias, Appl. Phys. B **64**, 387 (1997).
[32] F. J. Garcia-Vidal and J. B. Pendry, Phys. Rev. Lett. **77**, 1163 (1996).
[33] J. B. Smith and H. Ehrenreich, Phys. Rev. B **25**, 923 (1982).
[34] P. M. Echenique, J. M. Pitarke, E. V. Chulkov, and A. Rubio, Chem. Phys. **251**, 1 (2000).
[35] G. Manfredi and P.-A. Hervieux, Phys. Rev. B **70**, 201402(R) (2004).
[36] X. Liu, R. Stock, and W. Rudolph, *CLEO/IQEC and PhAST Technical Digest* (The Optical Society of America, Washington, DC, 2004), IWA4.